# Development of a Superconducting Magnet System for a Helicon Plasma Thruster

IEPC-2015-293／ISTS-2015-b-293

John J. Vitucci[1], Zachariah A. Brown[2], and Raymond J. Sedwick[3]
*University of Maryland, College Park, MD, 20740*

**A system design and analysis of the superconducting helicon thruster is presented. The design is of two subsystems, the superconducting magnet subsystem and thermal management subsystem. The superconducting magnet subsystem shows that using the combination of a solenoid and permanent magnet, a desirable magnetic field geometry for a helicon plasma can be supported. By adding a high-temperature type-II superconductor, the induced current in the superconductor from depowering the solenoid can sustain the same magnetic field geometry without the need to continuously power the electromagnet. The resulting field geometry is characterized by axial uniformity along the axis of the device at 200 G and a convergence upstream in a magnetic mirror configuration. The axial uniformity allows for the propagation of the helicon wave, where as the upstream convergence is intended to improve plasma confinement. In order to maintain cryogenic temperatures for the superconductor, the thermal management subsystem shows the capability of sustaining the critical temperature of the superconductor through the use of several insulating layers and a cryocooler. The cryocooler is to remove no more than 5 W, since a radiator is in place to remove the remaining 95 W provided by the plasma source.**

## Nomenclature

| | | |
|---|---|---|
| $a$ | = | Plasma source radius (m) |
| $B$ | = | External Magnetic field strength (G) |
| $c_p$ | = | Specific heat at constant pressure (J/kg K) |
| $E'_{ion}$ | = | Total ionization cost per ion/electron pair (eV) |
| $E_{ion}$ | = | Propellant first ionization energy (eV) |
| $e$ | = | Elementary charge (C) |
| $I$ | = | Solenoid current (A) |
| $k$ | = | Thermal conductivity (W/m K) |
| $L$ | = | Plasma source length (m) |
| $L_s$ | = | Solenoid length (m) |
| $m_e$ | = | Electron mass (kg) |
| $m_i$ | = | Ion mass (kg) |
| $n$ | = | Plasma density (1/m$^3$) |
| $n_n$ | = | Neutral density (1/m$^3$) |
| $n_s$ | = | Number of turns in solenoid |
| $p$ | = | First zero of the Bessel function $J_1$ |
| $\dot{P}_{rad}$ | = | Radiated power per volume (W/m$^3$) |
| $\dot{q}_r$ | = | Conducted power per area (W/m$^2$) |
| $r$ | = | Radial position (m) |
| $R_{ion}$ | = | Ionization rate (1/s) |
| $T$ | = | Temperature (K) |
| $t$ | = | Time (s) |
| $T_e$ | = | Electron temperature (eV) |

[1] Graduate Research Student, Department of Aerospace Engineering, jvitucci@umd.edu
[2] Undergraduate Research Student, Department of Aerospace Engineering
[3] Associate Professor, Department of Aerospace Engineering

| | | |
|---|---|---|
| $z$ | = | Axial position (m) |
| $\Gamma_s$ | = | Flux into plasma sheath (particles/m$^2$s) |
| $\mu_0$ | = | Permeability of free-space (N/A$^2$) |
| $\nu_e$ | = | Electron collision frequency (1/s) |
| $\rho$ | = | Density (kg/m$^3$) |
| $\omega_e$ | = | Electron cyclotron frequency (1/s) |

## I. Introduction

HELICON plasma thrusters have emerged as a viable propulsion mechanism for in-space applications due to high efficiency plasma generation at low power inputs[1]. In its simplest form, the helicon thruster consists of an externally applied magnetic field, helical antenna, plasma confining quartz tube, and RF power system. Most helicon thrusters have exhibited subpar performance[2,3,4], leading to designs that augment the stand alone thruster to increase performance. Williams[2] suggests that improvements beyond beam collimation and higher propellant utilization, such as increasing input power or implementing an ion acceleration stage, would be needed to increase efficiency beyond 30%. The most notable is the Variable Specific Impulse Magnetoplasma Rocket or (VASIMR)[5], which makes use of resonant ion cyclotron heating (ICH) stage to further heat the plasma before it is ejected from the rocket via a magnetic nozzle[6]. Other augmentations include the combination of a helicon plasma source with a gridded ion acceleration stage[7], and also the combination of a helicon ionization stage with a Hall thruster acceleration chamber[8].

Alternatively, Chen has proposed[9] modifications to the topology of the magnetic field from a permanent magnet. Choosing a magnetic field configuration in order to improve ion confinement could minimize one of the biggest power sinks in the helicon thruster; the loss of power to the plasma sheath along the tube boundaries as addressed by Fruchtman[10]. Typically, helicon thrusters require the external magnetic field to assist in the propagation of the helicon wave in addition to ion confinement[11]. The strength of the magnetic field also directly determines the maximum plasma density that can be supported by the plasma, which saturates for magnetic fields in excess of 1000 G[11,12]. While there is little to suggest the strength of the axial magnetic field directly contributes to ion acceleration, there has been evidence demonstrating that its geometry is of greater influence[13]. It has been shown[14,15,16,17] that helicon wave propagation is impeded in the presence of non-uniformities and nulls in the magnetic field geometry. This supports the convention of a uniform magnetic field along the axis of a cylindrical plasma source. At the exit of the thruster, a diverging magnetic field has been shown to support the formation of the naturally occurring acceleration mechanism.

## II. Methodology

A novel approach to modifying the topology of the externally applied magnetic field is through the use of the Meissner effect[18]. This results in a design for a superconducting helicon thruster consisting of two subsystems, the superconducting magnet subsystem and the thermal management subsystem. Based on the previous studies mentioned above, we impose two conditions on the design of the superconducting magnetic subsystem:

1. Axial uniformity downstream of the helical antenna to ensure the propagations of the helicon wave throughout the ionization and accelerations regions within the helicon plasma.
2. Magnetic mirror[19] to confine the plasma, increase ion residence times, and also to reduce power losses to the upstream plasma sheath.

The principle idea is that of an ideal superconducting tube capped at one end by a permanent disk magnet. Once the superconductor reaches its critical temperature, the magnetic flux will be expelled from the material and wrap sharply around the open end of the tube to reconnect with the opposite pole of the magnet. A qualitative model of this can be seen in Fig. 1. The sharp divergence at the exit is also hypothesized to provide a more collimated beam due to a more rapid detachment of the plasma[20]. Experimental implementation would require the use of a low-temperature type-I superconductor since they exhibit perfect diamagnetism and will completely expel magnetic flux within the material[21]. The difficulty lies in developing a cooling system capable of reaching temperatures in the range of 1 – 20 Kelvin, which is typically required to reach the critical temperatures of these materials.

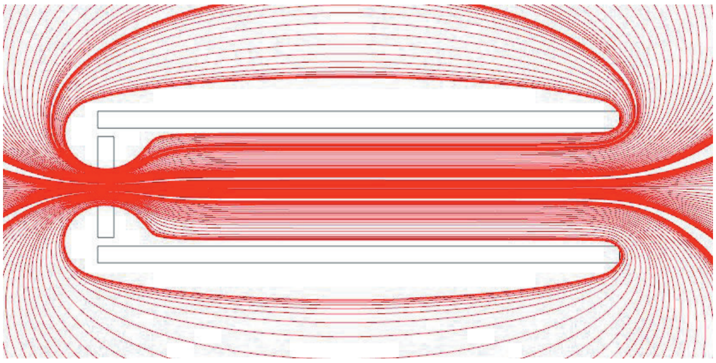

**Fig. 1. COMSOL simulation of magnetic field lines from a permanent disc magnet placed inside the end of the HTS tube while superconducting[21].**

To avoid the challenge of achieving such low temperatures, an alternative approach is to use high-temperature type-II superconductors. These typically have much higher critical temperatures in the range of 90 – 130 K[21]. The difficulty in utilizing this class of superconductors lies in its mixed, or vortex, state[22], which allows for partial penetration of magnetic flux when the external magnetic field dominates the Meissner current on the materials surface[23]. This results in a phenomenon known as flux pinning, where magnetic flux becomes trapped within supercurrent vortices, preventing the flux from moving within the material, and shielding the other regions of the superconductor from the trapped magnetic flux[24]. This effect occurs when magnetic flux is present within the material prior to achieving the critical temperature, and poses a design challenge in that the flux must be removed before reaching the critical temperature.

In order to maintain the critical temperature of the superconductor, a thermal management subsystem must also be designed. For practical application as an in-space platform, we impose two conditions on this subsystem:

1. Maintain cryogenic temperatures below the critical temperature of the superconductor.
2. Insulate the cryogenic region from heat generated by the plasma, and radiate excess thermal power.

This can be achieved through a combination of conductive layers to intercept heat from the plasma and conduct it to a radiator, and insulating layers to prevent the heat from reaching the cryogenic region. The helical antenna introduces an additional challenge. Since the plasma source will be within the confines of the superconducting magnet subsystem, the power leads must be run in the axial direction. This requires electrically insulating layers in order to prevent the RF power from conducting to other regions of the thermal management subsystem.

## III. Superconducting Magnet Subsystem

### A. Principles of Operation

Using a flux conservation approach, one can use a combination of electromagnets, permanent magnets, and high-temperature type-II superconductors to achieve a desirable magnetic field configuration, while also minimizing the total power into the system by eliminating the need to continuously power the electromagnet. A solenoid is used to satisfy the first criterion of the axially uniform magnetic field, and a high-temperature type-II superconducting tube is located coaxially within the solenoid as seen in the schematic (Fig. 2). The solenoid initially generates the magnetic field, at which point the superconductor is cooled to below its critical temperature by feeding liquid nitrogen into an aluminum vessel containing the superconductor. The axial magnetic field strength inside the solenoid is found by using Ampere's Law, $B = \frac{\mu_0 n_s I}{L_s}$. Here, $n_s$ is the number of turns, $I$ is the current in the solenoid, and $L_s$ is the solenoid's length. Once the critical temperature has been reached, the solenoid can be switched off. A current will be induced in the superconductor according to Lenz's Law that is not subject to resistance within the material. The magnitude of this current is equal to the product of the number of turns in the solenoid and the current in the solenoid windings. If the superconductor is treated as though it were a solenoid itself, then the axial magnetic field strength will be identical to what was produced with the solenoid (provided the superconductor and solenoid have the same length), without the need to continuously power the solenoid. To generate the upstream convergence, a permanent ring magnet will be placed outside of the upstream end of the superconductor housing, and coaxial with the superconductor. This can also be seen in Fig. 2.

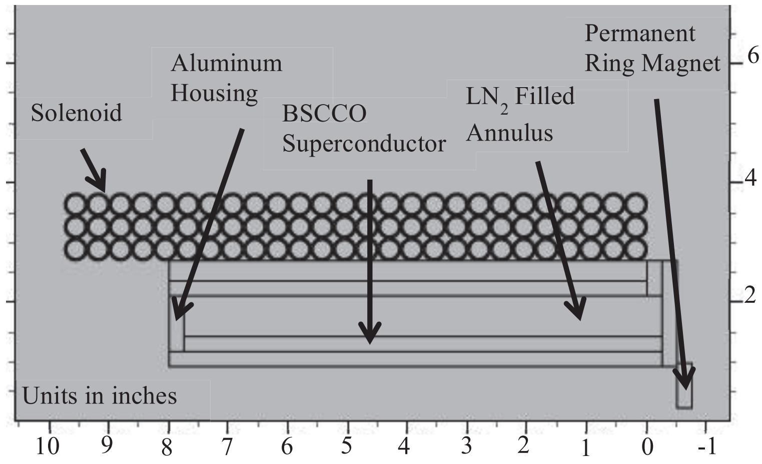


**Fig. 2. Axi-symmetric superconducting helicon thruster schematic.**

### B. Computational Modeling and Experimentation

In order to visualize and predict the strength and shape of the magnetic field, a model using COMSOL Multiphysics was developed. First, the model was used to predict the magnetic field using the combination of the solenoid and the permanent magnet. This model was then verified with the experimental results before modeling the scenario with the superconductor and the permanent magnet. The COMSOL model was designed to match the experimental system to allow for direct comparison with the measured field. Originally[13], a permanent magnet with inner diameter 1.5” and outer diameter 3” was used, however, in order to improve the magnetic mirror effect upstream, a smaller permanent magnet was implemented. The new magnet is 0.5” inner diameter and 2” outer diameter. The model accounts for the magnetization in the permanent magnet and the contribution from the solenoid by using a 2D axi-symmetric model, and can be seen in Fig. 3.

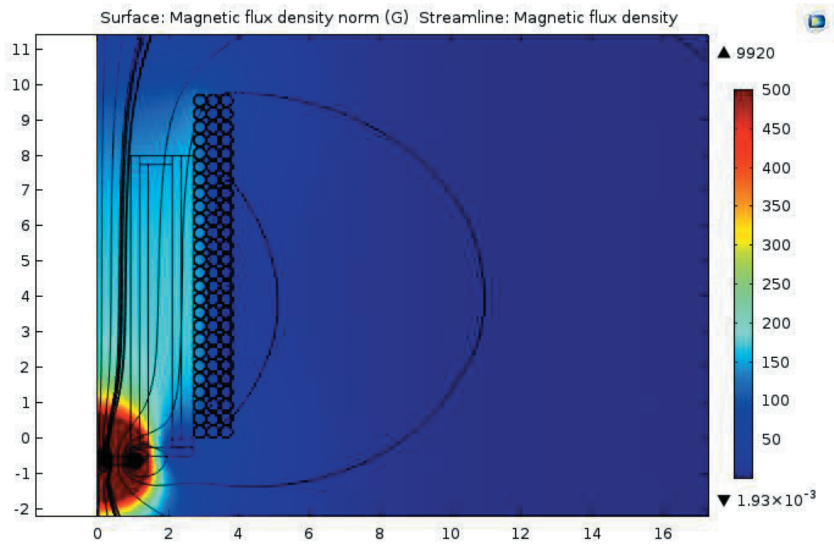


**Fig. 3. COMSOL model of solenoid and permanent ring magnet field.**

It is important to note that this geometry alone satisfies the two criteria for the superconducting magnet subsystem. The design maintains axial uniformity along the length of the device, while also providing the upstream convergence. This is especially evident when looking at the on-axis cut of the magnetic flux density, and can be seen in Fig. 4. The next step was to verify that the model accurately predicts the magnetic field geometry for the solenoid and permanent magnet case. To do this, the experimental setup was constructed as seen in Fig. 2. A magnet field mapping apparatus was constructed using aluminum 80/20 beams. A pair of Velmex bi-slides was used to translate the magnetic field probe within the open volume inside of the aluminum housing. The power to the solenoid was provided by a set of Nickel-Cadmium D-cell batteries at about 64 A of current and a potential drop over the solenoid of about 2.4 V. The current into the solenoid was monitored using a Rogowski coil, in order to verify a steady current was maintained throughout the magnetic field sweep. Since the solenoid is about 78 turns of 3/8" insulated copper tubing, water from a chiller is pumped through the tubing in order to actively cool the solenoid. The complete experimental setup can be seen in Fig. 5. A Labview VI was written to measure the magnetic flux density in the axial direction and log the measurements for a two-dimensional sweep. The data was then plotted using Matlab, where the results are shown in Fig. 4 along with the results from the COMSOL model. Very good agreement is observed between the experimental and the computational results, verifying the accuracy of the COMSOL Multiphysics model. Additionally, the magnetic field strength along the axis is low enough to avoid exceeding the critical current limitation of the superconductor.

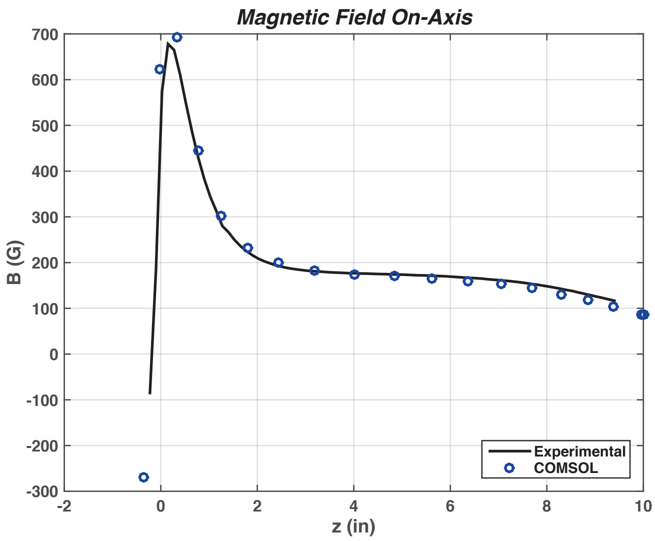


**Fig. 4. On-Axis magnetic flux density for superconducting magnet subsystem without superconductor.**

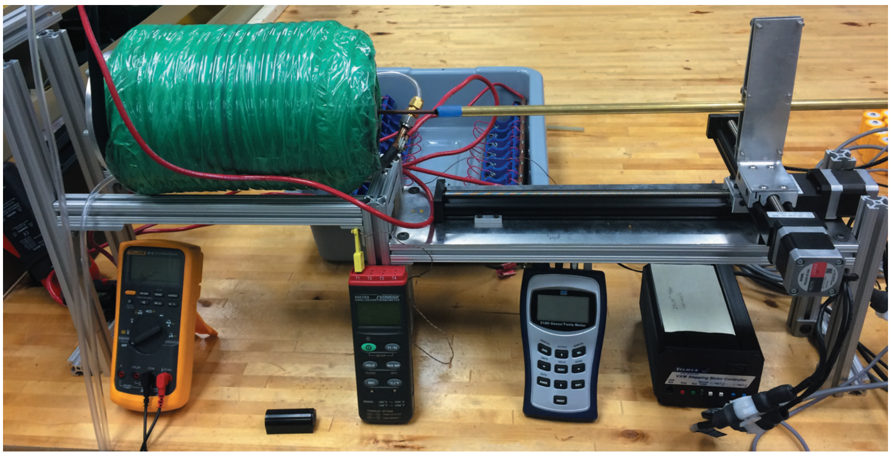

**Fig. 5. Solenoid and magnetic field mapping apparatus.**

The next step after verifying the computational model for the solenoid and permanent magnet case is to model the same configuration, but using the superconductor in place of the solenoid. Since COMSOL cannot account for a change in material properties of the superconductor and the depowering of the solenoid, the superconductor and permanent magnet was modeled as a steady-state system. In this case, the induced current density in the solenoid is assumed to be the same current density in the solenoid. The superconductor is given an external current density and modeled in the same manner as the solenoid. Since the solenoid of greater length than the superconductor, it is expected that at the exit of the superconductor, the field will drop off at a different position than seen in the solenoid. This is seen in the COMSOL model, and is readily observed in Fig. 6. This plot includes the same information from Fig. 4, but now includes the model of the superconductor and permanent magnet case for direct comparison. Very good agreement can be seen up to the exit plane of the superconductor, as expected. It is important to note that this configuration still maintains the two criteria for the superconducting magnet system in that it exhibits a uniform field along the axis of the superconductor with a convergence upstream in a magnetic mirror configuration. This configuration will be tested experimentally at a later date, and comparison to this model will be disseminated in a future paper.

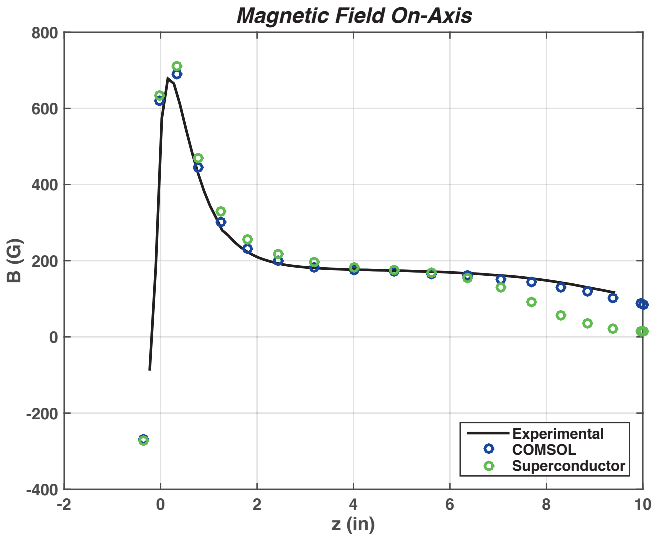


**Fig. 6. On-axis magnetic flux density for superconducting magnet subsystem, with and without superconductor.**

## IV. Thermal Management Subsystem

### A. Power Flow Analysis

In a practical application of the superconducting helicon thruster, the cryogenic temperatures must be maintained in a closed-loop system. For laboratory testing, the solution is simpler in that an open-loop liquid nitrogen cooling system can be applied. This study assumes that the primary contribution of thermal energy to the system comes from the plasma column, and that the heat initially generated by the solenoid is removed prior to its depowering once the critical temperature of the superconductor has been reached. The primary contributions from the plasma column are the conducted and radiated powers that result from maintaining the plasma. The total conducted and radiated powers are calculated and the insulated layers separating the plasma column and the cryogenic region are determined based on the power to be removed by a cryocooler. A radiator must then remove any excess heat. The area of the radiator is uniquely determined based on the power to be radiated and its temperature. Additionally, once these powers are determined, the total RF power required to maintain the plasma column can be calculated.

The equations for the radiated power per volume and conducted power per area are as follows[25]:

Radiated Power:

$$\dot{P}_{rad} = e(E'_{ion} - E_{ion})nn_n R_{ion} \qquad \left[\frac{W}{m^3}\right] \tag{1}$$

Conducted Power:

$$q_r = \left(2 + \frac{1}{2} ln\left(\frac{m_i}{2\pi m_e}\right)\right) eT_e\Gamma_s \qquad \left[\frac{W}{m^2}\right] \tag{2}$$

Here, we assume argon plasma with electron temperature of 5 eV, plasma density of $5(10^{17})$ m$^{-3}$, 40 cm plasma source length, and 1.64 cm source radius. With this, the total ionization cost, neutral density, ionization rate, and particle flux into the sheath can be calculated. The study in Ref. [26] uses these equations and then calculates the distribution of the radiative heat flux to the back wall and lateral wall. Proper discretization yields a radiated power flux to the back and lateral walls as shown in Fig. 7 and Fig. 8. The open downstream boundary is not accounted for as any losses here are contributing to the thrust rather than heating the device.

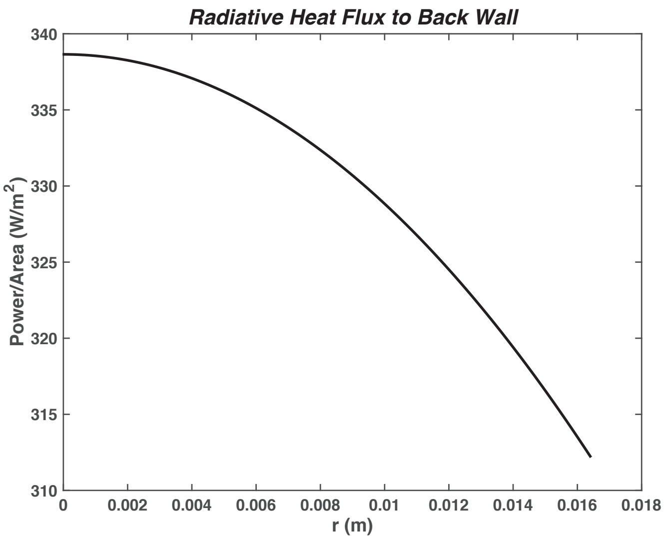


**Fig. 7. Radiative heat flux distribution to the upstream wall.**

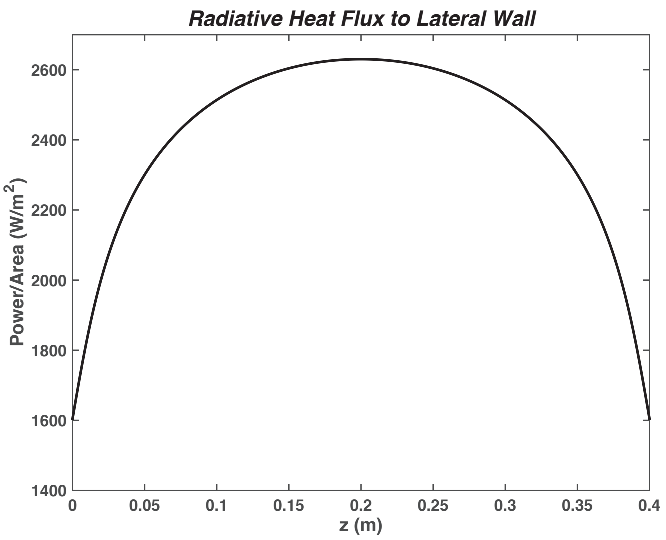


**Fig. 8. Radiative heat flux distribution to the lateral wall.**

By integrating these two plots over the area of the back wall and lateral wall, respectively, we find that the power radiated to the lateral wall dominates the power radiated to the back wall. The total radiated power is 100 W. The conducted power is only assumed to be through the lateral wall since the upstream convergence yields a negligible contribution of conducted power. Similarly, the conducted power density to the lateral wall can be integrated over the total area, yielding a total conducted power of 230 W. Collecting the power lost to conduction, radiation, and total cost of ionization per ion/electron pair (120 eV for Argon plasma), yields a total RF input power of about 450 W in order to sustain the plasma source. Since this study assumes a general plasma source, it does not account for the efficient plasma generation of the helicon wave-particle interaction, thus making this a worst-case scenario.

Additionally, this does not account for the presence of the magnetic field, which helps confine the ion flux to the wall and thus reducing the conducted power to the lateral wall.

Assuming that the particle flux to the lateral wall is equal to that due to ambipolar diffusion[26], the particle flux in Eq. (2) can be substituted with the following:

$$\Gamma_s = \frac{T_e \nu_e}{m_e \omega_e^2} \frac{p}{a} n J_1 \left(\frac{pr}{a}\right) \cos\left(\frac{\pi z}{L}\right) \tag{3}$$

The only required condition for this to hold is that the electrons are magnetized, which can readily be seen using an on-axis magnetic field strength of 200 G. By taking the radial position to be at the boundary, $r = a$, and integrating over the axial direction yields a conducted power four orders of magnitude lower than without accounting for the magnetic field. This now results in a total power of 100 W that must be removed in order to maintain cryogenic temperatures. It can now be shown that the total RF input power to maintain the plasma source is 220 W, which is still an over-assumption since the efficient ionization nature of the helicon source is not accounted for. This can reduce the total ionization cost as low as twice the first ionization energy of the gas.

### B. Subsystem Design

The thermal management subsystem is of four distinct insulating layers, a copper radiator, and a cryocooler. The insulating layers serve the purpose of thermally isolating the cryogenic region and also electrically isolating the helical antenna leads. Since the plasma source tube, simply made of quartz, is confined within the superconductor housing, the antenna leads must be fed into the system along the axis and cannot come into electrical contact with any other conducting layers. This is especially important since the first layer outside of the source tube is a 0.16 cm conformal copper layer that intercepts the radiated heat and readily conducts it to the radiator. The next layer is a 0.08 cm Kapton layer, which electrically insulates and separates the 0.16 cm thick antenna leads from the conformal copper layer and helical antenna. Another 0.08 cm Kapton layer is wrapped around the antenna leads to ensure they are electrically isolated from the conformal copper layer and the copper antenna. This now leaves a 0.08 cm vacuum gap separating the final Kapton layer and the aluminum housing wall. The conformal copper layer is connected to a cone shaped radiator at the exit of the thruster. In order to radiate the remnant power to be removed by the cryocooler, the final Kapton layer is selected to be aluminized (emissivity 0.03) on the side facing the inner wall of the aluminum housing. A schematic, not drawn to scale, can be seen in Fig. 9.

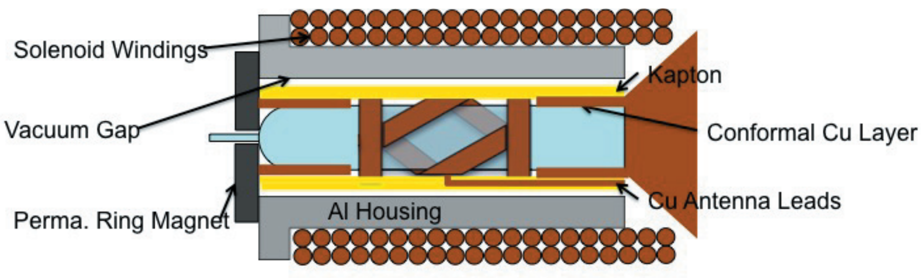


**Fig. 9. Schematic of thermal management design for the superconducting helicon thruster.**

The area of the radiator can be found since the temperature of the conformal copper layer can be calculated and the required radiated power is known. By setting a maximum allowable power of 5 W to be removed by the cryocooler, 95 W must now be removed by the radiator. In order for the aluminized Kapton layer to radiate 5 W of power, its temperature can be uniquely determined since its area is known. This results in a temperature of 474 K. The emissivity of the radiator is chosen to be 0.9, corresponding to a rough, black matte paint coating on the copper. To calculate the temperature of the conformal copper layer, the one-dimensional heat transfer equation must be solved for each layer:

$$\frac{\partial T}{\partial t} = \frac{k}{c_p \rho}\left[\frac{1}{r}\frac{\partial}{\partial r}\left(r\frac{\partial T}{\partial r}\right) + \frac{\partial^2 T}{\partial z^2}\right] + \frac{\dot{q}}{c_p \rho} \tag{4}$$

Doing so results in the temperature profile seen in Fig. 10, and yields a temperature of 477 K for the copper layer and the radiator. Now that the radiated power and temperature are known, the Stefan-Boltzmann law can uniquely determine the size of the radiator. To radiate the remaining 95 W at 477 K, the radiator area must be 0.036 m$^2$. To further reduce the size of the radiator, excess power can be used to preheat the propellant. This is especially attractive for water vapor propellant applications, to which this system lends itself well.

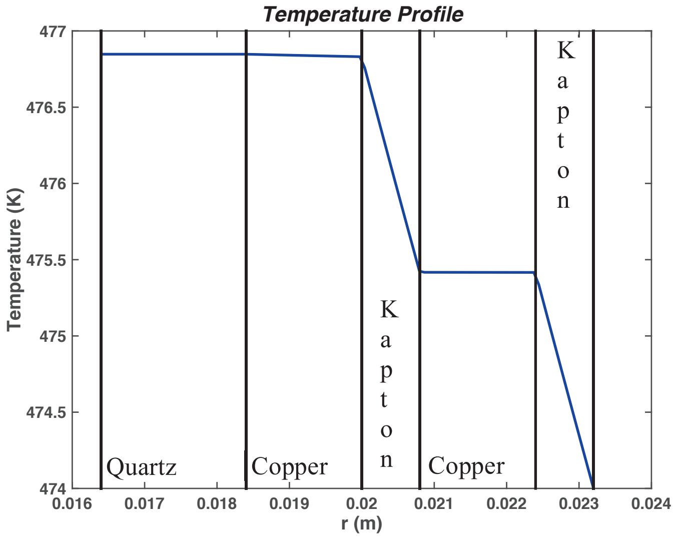


**Fig. 10. Temperature profile for thermal management subsystem insulating layers.**

## V. Conclusion and Future Work

A system design for a superconducting helicon thruster has been presented. The superconducting magnet subsystem has shown the capability of satisfying the two main criteria through the combination of a solenoid, permanent magnet, and high-temperature type-II superconductor. The superconductor is capable of sustaining the magnetic field generated by the solenoid without the need of continuous power. The resulting magnetic field geometry exhibits the axial uniformity and upstream convergence demanded of it. It has also been shown that the combination of a radiator, cryocooler, and insulating layers can maintain the critical temperature of the superconductor. The radiator removes the bulk of the radiated power from the helicon plasma source, and the cryocooler is capable of removing the remainder. Combining the two subsystems results in a viable in-space thruster that reduces the required power for operation, increases plasma generation efficiency due to the efficient nature of the helicon thruster, and also offers an ideal platform for water vapor propellant applications.

Future work includes the magnetic field mapping of the superconductor and permanent magnet case. Once this information has been collected, it will be compared with the COMSOL model presented in this paper. These results will be disseminated in a future paper. Finally, the complete superconducting magnet subsystem will be integrated with the baseline helicon thruster for performance comparison. To maintain the cryogenic temperatures in the laboratory setting, an open-loop liquid nitrogen setup will be used to avoid the complexity of the in-space application design presented in this paper. Since the focus is on the performance of the thruster compared to the baseline helicon thruster, it is not vital to integrate the closed-loop system.

## Acknowledgments


This work was supported in part by a NASA Office of the Chief Technologist's Space Technology Research Fellowship.


## References


[1]Boswell, R. W., "Very Efficient Plasma Generation by Whistler Waves Near the Lower Hybrid Frequency," *Plasma Phys. And Controlled Fusion*, Vol. 26, No. 10, 1984, pp. 1147-1162.

[2]Williams, L. and Walker, M., "Thrust Measurements of a Helicon Plasma Source," Paper AIAA-2011-5893, *47th AIAA/ASME/SAE/ASEE Joint Propulsion Conference & Exhibit,* San Diego, CA, 2011.

[3]Pottinger, S., Lappas, V., Charles, C., and Boswell, R. W., "Performance Characterization of Helicon Double Layer Thruster Using Direct Thrust Measurements," *J. Phys. D: Appl. Phys.*, Vol. 44, 2011, p. 235201.
[4]Takahashi, K., et al., "Direct Thrust Measurements of a Permanent Magnet Helicon Double Layer Thruster," *Appl. Phys Lett.*, Vol. 98, 2011, p. 141503.
[5]Chang-Díaz, F. R., "The VASIMR Rocket," *Sci. Amer.*, Vol. 283, 2000, pp. 90-97.
[6]Chang-Díaz, F. R., "An Overview of the VASIMR Engine: High Power Space Propulsion with RF Plasma Generation and Heating," *Radio Frequency Power in Plasmas*, 14th Topical Conference, Oxnard, CA, AIP Conference Proceedings, Vol. 595, 2001, p. 3.
[7]Williams, L. and Walker, M., "Initial Performance Evaluation of a Gridded Radio Frequency Ion Thruster," *AIAA Journal of Propulsion and Power*, Vol. 30, No. 3, 2014, pp. 645-655.
[8]Peterson, P., et al., "Performance and Plume Characterization of a Helicon Hall Thruster," Paper IEPC-2011-269, *The 32nd International Electric Propulsion Conference*, Wiesbaden, Germany, September 11-15 2011.
[9]Chen, F. F., "Permanent Magnet Helicon Source for Ion Propulsion", *IEEE Trans. Plasma Sci.,* Vol. 36, No. 5, 2008, pp. 2095-2110.
[10]Fruchtman, A., "Neutral Depletion in a Collisionless Plasma", *IEEE Trans. Plasma Sci.,* Vol. 36, No. 2, 2008, pp. 403-413.
[11]Sinenian, N., "Propulsion Mechanisms in a Helicon Plasma Thruster," *Master's Thesis*, Department of Nuclear Science and Engineering and Department of Electrical Engineering and Computer Science, Massachusetts Institute of Technology, Cambridge, MA, 2008.
[12]Chen, F. F., "Plasma Ionization by Helicon Waves," *Plasma Phys. and Controlled Fusion*, Vol. 33, No. 4, 1991, pp.339-364.
[13]Vitucci, J. J. and Sedwick, R. J., "Improved Superconducting Magnet System to Reduce Upstream Boundary Losses in a Helicon Plasma Thruster," Paper AIAA 2014-3405, 50th AIAA/ASME/SAE/ASEE Joint Propulsion Conference and Exhibit, San Jose, CA, July 2014.
[14]Chen, F. F., "Experiments on Helicon Plasma Sources," *J. Vac. Sci. Technol.*, Vol. 10, No. 4, 1992, pp. 1389-1401.
[15]Shamrai, K., et al., "Compact Helicon Plasma Source with Permanent Magnets for Electric Propulsion Application," Paper AIAA-2006-4845, *42nd AIAA/ASME/SAE/ASEE Joint Propulsion Conference & Exhibit,* Sacramento, CA, 2006.
[16]Charles, C. and Boswell, R. W., "Current-Free Double-Layer Formation in a High-Density Helicon Discharge," *Appl. Phys. Lett.,* Vol. 82, No. 9, 2003, pp. 1356-1358.
[17]Plihon, N., Chabert, P., and Corr, C.S., "Experimental Investigation of Double Layers in Expanding Plasmas," *Physics of Plasmas*, Vol. 14, No. 1, 2007, p. 013506.
[18]Forrest, A. M., "Meissner and Ochsenfeld revisited", *Eur. J. Phys.*, Vol. 4, 1983, pp. 117-120.
[19]Helffer, B. and Morame, A., "Magnetic Bottles in Connection with Superconductivity," *Journal of Functional Analysis*, Vol. 185, 2001, pp. 604-680.
[20]Vitucci, J. J. and Sedwick, R. J., "Development of a Superconducting Helicon Thruster," Paper AIAA 2012-3866, 48th AIAA/ASME/SAE/ASEE Joint Propulsion Conference and Exhibit, Atlanta, GA, July-August 2012.
[21]Wilson, A., Vitucci, J. J., and Sedwick, R. J., "Flux Tailoring of a Permanent Magnet Field with a High Temperature Superconducting Tube for a Helicon Plasma Source," *IEEE Trans. Appl. Supercond.*, Vol. 22, No. 5, 2012, pp. 3900705.
[22]Abrikosov, A., "Type II Superconductors and the Vortex Lattice", Nobel Lecture, 2003, pp. 59-67.
[23]Sheahen, T., *Introduction to High-Temperature Superconductivity*. New York, NY: Springer, 1994, p. 26.
[24]Kittel, C., *Introduction to Solid State Physics*, Hoboken, NJ: Wiley, 2005, pp. 259-293.
[25]Navarro-Cavallè, et al., "Design of Helicon Plasma Thruster subsystems," Paper AIAA 2014-3699, 50th AIAA/ASME/SAE/ASEE Joint Propulsion Conference and Exhibit, San Jose, CA, July 2014.
[26] Fruchtman, A., "Ambipolar and nonambipolar cross-field diffusions," *Plasma Sources Sci. Tech.*, Vol. 18, 2009, p. 025033.